Chapter-4

Biogenic AuNPI3Cs exhibit antineoplastic potential against human leukemia and breast cancer cell lines through the induction of apoptosis and oxidative stress

4.1 Introduction

4.2 Materials and methods

4.3 Results

4.4 Discussion

4.5 Conclusion

Abstract

Nanotechnology has provided an opportunity to explore new possibilities that conventional technologies have been unable to make an impact for prevention, and therapy of cancer. This study reports the *in vitro* antineoplastic activity of gold nanoparticles from indole-3-carbinol (AuNPI3Cs) against human T cell leukemia cell line (Jurkat cells) and breast cancer, MCF-7 cells. AuNPI3Cs have shown reduced cell viability in Jurkat and MCF-7 cells with IC_{50} concentration of 5.55 and 4.9 µg/ml respectively. AuNPI3Cs increased ROS generation and induced apoptosis by elevating chromatin condensation, DNA fragmentation, cell cycle arrest, expression of pro-apoptotic proteins and mitochondrial dysfunction in Jurkat and MCF-7 cell. AuNPI3Cs treatment disrupted the regular reorganization of actin filaments in MCF-7 cells. The findings confirm that AuNPI3Cs prompted an antineoplastic effect in breast cancer and AuNPI3Cs may be a new drug candidate against leukemia and breast cancer in future.

4.1 Introduction

Cancer is the third leading cause of death in developing countries. According to WHO, cancer now represents approximately 13.3% of deaths and are expected to rise by at least 50% worldwide over the next 20 years (Seigel et al., 2012). Cancer is a complicated genetic disease caused mainly by environmental factors and its treatment is usually by a combination of numerous modalities.

4.1.1 Apoptosis

Cell death, mainly apoptosis, is probably one of the most widely-studied subjects among cell biologists. The term "apoptosis" is derived from the Greek words 'apo' and 'tosis' meaning 'dropping off' and denotes the falling of leaves from trees in autumn. Nuclear chromatin condensation and fragmentation are morphological characteristics of apoptosis, which manifestated by rounding up of the cell, reduction in cellular volume (pyknosis) and retraction of pseudopodes (Kroemer et al., 2005).

Generally, three major biochemical changes are seen in apoptosis: 1) activation of caspases, 2) breakdown of DNA and protein, and 3) membrane alterations and it is recognized by phagocytic cells (Kumar et al., 2010). In early apoptosis, phosphatidylserine (PS) is flipped out from the inner layer to the outer layer of cell membrane. Macrophages early recognize the dead cells resulting in phagocytosis but do not release proinflammatory cellular components. Then a characteristic breakdown of DNA into large 50 to 300 kilobase pieces occurs (Vaux and Silke, 2003). Endonucleases cause internucleosomal cleavage of DNA into multiple oligonucleosomes.

4.1.2 Mechanism of apoptosis

Understanding the mechanisms of apoptosis helps to know the pathogenesis of some diseases caused by disordered apoptosis and may also help in the drug development that target certain apoptotic genes or pathways. Caspases are both the initiators and executioners of apoptosis and there are three pathways of caspase activatation. The two usually designated initiation pathways are the intrinsic mitochondrial and extrinsic (or death receptor) pathways of apoptosis (Figure 1). Both pathways finally lead to a common execution phase of apoptosis. The intrinsic endoplasmic reticulum pathway is a third initiation pathway which is less well known (Wong, 2011).
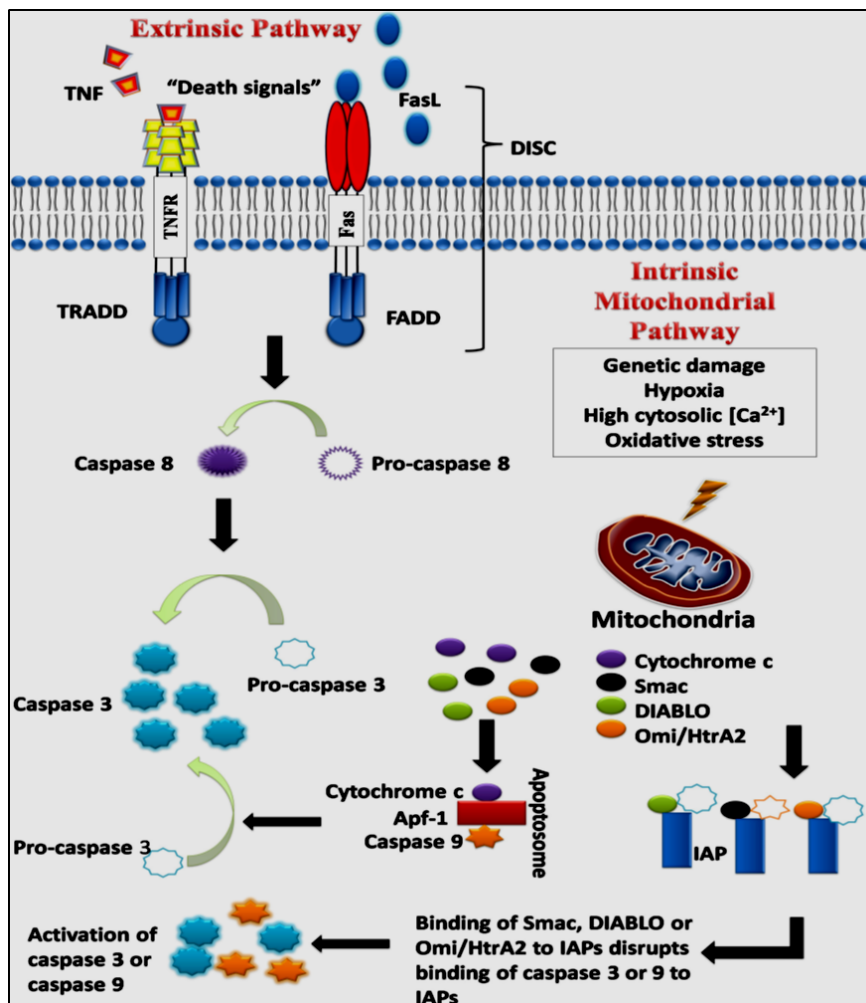

Figure 4.1 The intrinsic and extrinsic pathways of apoptosis

Intrinsic pathway is mainly controlled by Bcl -2 family such as Bax, Bcl-2 and Bak, Bcl-xl (Wong, 2011). Bcl-2 family regulate the release of proteins between the inner and outer membrane of mitochondria and it activates caspase proteases and promotes phagocytosis of dead cells (Wang and Youle, 2016). Apoptotic signal transforms Bax into mitochondrial oligomers which becomes activated and damaged mitochondria. When death ligands bind to a death receptor, the extrinsic death receptor pathway starts. Death receptors is the type 1 TNF receptor (TNFR1) and a related protein called Fas (CD95) and their ligands are called TNF and Fas ligand (FasL) respectively (Hengartner, 2000). These death receptors having an intracellular death domain recruits adapter proteins such as TNF receptor-associated death domain (TRADD) and Fas-associated death domain (FADD), as well as cysteine proteases like caspase 8. The apoptosis involves the activation of a series of caspases.

The upstream caspase for the intrinsic pathway is caspase 9 while that of the extrinsic pathway is caspase 8. The intrinsic and extrinsic pathways converge to caspase 3. Caspase 3 then cleaves the inhibitor of the caspase-activated deoxyribonuclease, which is responsible for nuclear apoptosis (Ghobrial et al., 2005)
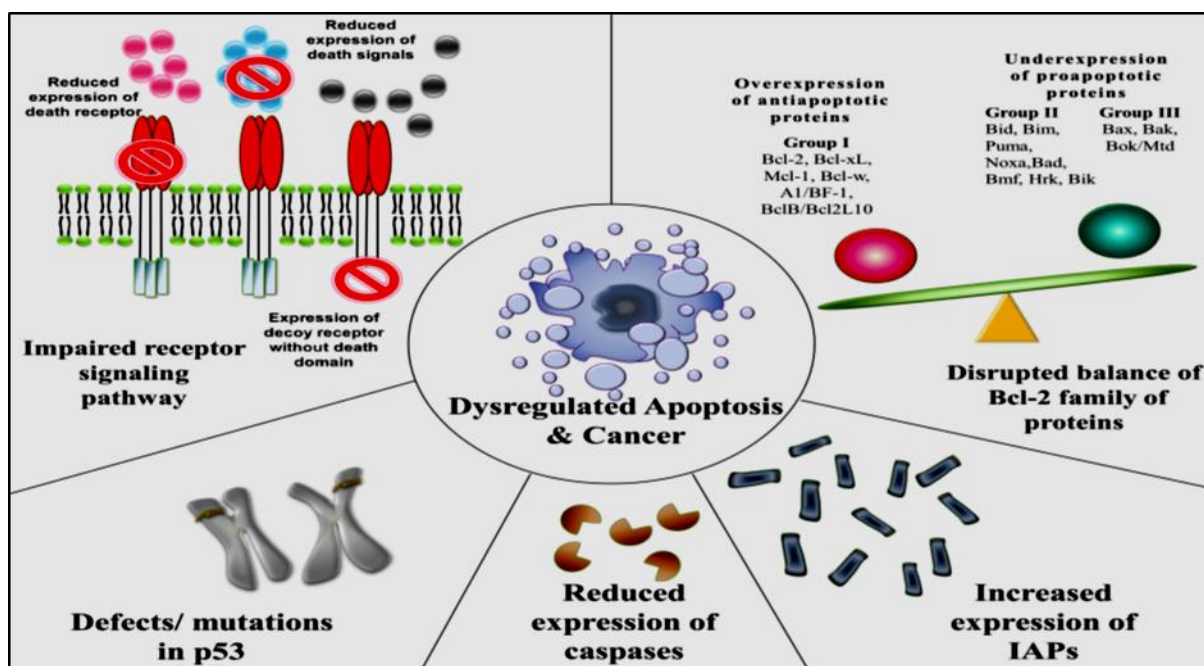
Figure 4.2 Mechanism of apoptosis

4.1.3 Oxidative stress and apoptosis

Apoptosis can be activated by oxidative stress which is caused by excessive production of reactive oxygen species (ROS) such as hydrogen peroxide H_2O_2, hydroxyl radical $OH\bullet$, superoxide $O_2^{-}\bullet$ and peroxyl $RO\bullet$. ROS are repetitively generated as a consequence of aerobic respiration (Halliwell and Cross, 1994). ROS are also involved in a variety of normal cellular processes. However, excessive formation of ROS has been implicated in various diseases such as cancer, diabetes and neurodegenerative disorder (Chen et al., 2012). Oxidative stress restricting from chronic inflammation is well known to be involved in carcinogenesis (Wiseman and Halliwell, 1996). Oxidative DNA lesions and nitrative DNA lesions were detected in cancer cells and inflammatory cells (Ma et al., 2008). DNA double-

strand breaks and engagement of the DNA damage which were associated with formation of ROS and were reversed by antioxidants (Gruhne et al., 2009).

Apoptosis is frequently convoyed by the generation of reactive oxygen species (ROS), resulting in part from cytochrome c departure from mitochondria and attendant disruption of electron transport with enhanced generation of one-electron-reduced species of molecular oxygen within the cell (Chandra et al., 2000). ROS offers important candidates for final common mediators of apoptosis. A specific role for ROS for the execution of the apoptosis has not yet been established.

4.1.4 Leukaemia

Abnormal proliferation of blood cells and blood forming organs lead to a malignant condition commonly known as leukaemia. The beginning of leukaemia may be acute or chronic. Cells belonging to both myeloid and lymphoid lineage are produced from haematopoietic stem cells during the process of haematopoiesis (Kondo, 2010). There are various types of leukaemia. The four main types include Acute Myelogenous Leukaemia (AML), Chronic Myelogenous Leukaemia (CML), Acute Lymphocytic Leukaemia (ALL) and Chronic Lymphocytic Leukaemia (CLL) (Redaelli et al., 2003). There are some other forms of leukaemia which are normally infrequent; T-cell prolymphocytic leukaemia, large granular lymphocytic leukaemia and adult T-cell leukaemia.

Jurkat cell is an immortalized cell line of human T lymphocyte cells. The cell lines are used to study acute T cell leukemia. Jurkat cell line was established in the late 1970s and obtained from the peripheral blood of a 14-year-old boy with T cell leukemia.

4.1.5 Breast Cancer

Malignancy of breast cancer starts in the breast epithelium cells and occurs particularly in women (Alison 2001). According to the Times of India, every year in India, 1, 00,000–1, 25,000 new breast cancer cases are occurred (12 Oct. 2012) In 2025, this statistical number is expected to be double. About half of all breast cancers are noticed in an advanced stage (Stapleton et al., 2011).

Though 20%-25% of breast cancer patients tolerate a positive family history but only 5%-10% of breast cancer cases expose an autosomal dominant inheritance (Margolin et al., 2006). Genetic predisposition alleles have attended clinical significance (Lalloo and Evans, 2012). High-risk predisposition alleles conferring a 40%-85% lifetime risk of developing breast cancer include BRCA1 and BRCA2 mutations, mutations in TP53 gene resulting in Li-Fraumeni syndrome, PTEN resulting in Cowden syndrome, STK11 causing Peutz-Jegher's syndrome, Neurofibromatosis (NF1) and (CDH-1) E-Cadherin (Sharif et al., 2007). Half of the breast cancer predisposition syndromes are associated with mutations in BRCA1 and BRCA2.

Breast cancer, a clinically heterogeneous disease, is classified into three groups. One is ER/PR positive, the second one is ER negative or HER-2 positive and the third is triple negative (ER, PR and HER-2 negative).

MCF-7 is a breast cancer cell line isolated in 1970 from a 69-year-old Caucasian woman. MCF-7 is the acronym of Michigan Cancer Foundation-7, referring to the institute in Detroit where the cell line was established in 1973 by Herbert Soule and co-workers (Soule et al., 1973).

4.1.6 Herbal therapy in leukemia and breast cancer

Nowadays basically chemotherapy, surgery, and radiation altogether are the standard treatment procedures for cancer (American Cancer Society, 2016). However, all these mode of treatment are seen to be associated with side effects and drug resistance, particularly at higher doses. Furthermore, majority of anticancer drugs extensively kill both cancer cells as well as normal cells, and these facts require the search for novel therapies. Leukaemia being a systemic disease, its treatment and cure depends on chemotherapy rather than surgery (Shacter et al., 2000). Due to toxicity in normal cell, recently chemotherapy does not require for its curing.

Triumfetta welwitschii extract was shown to have anti-proliferative activity against Jurkat T cells (Moyo and Mukanganyama, 2015).

Various active compounds derived from medicinal plants have been assessed for their efficacy and tolerability in the treatment of human breast cancer. Some of these plant species, including *Taxus brevifolia*, *Taxus baccata*, *Podophyllum peltatum*, *Camptotheca accuminata*, and V*inca rosea* have well-recognized anticancer activity in breast and other human malignancies (Mans et al., 2000). Earlier, paclitaxel analogs have provided a natural source and were used mostly in breast cancer and Kaposi sarcoma (Crag and Newman, 2005).

4.1.7 Gold nanoparticles on leukaemia and breast cancer

Chemotherapy is existing treatment for cancer but still it shows low specificity and is limited by dose limiting toxicity. It is a challenge to find the therapy and nanodrugs for the treatments of various types of cancer. So, conventional methods require the targeted drug delivery which is more effective and less harmful. Nanomaterials are expected hopefully to develop cancer diagnosis and therapy (Rosarin et al., 2012). Recently biosynthesized gold

nanoparticles used in anticancer therapy for several types of cancer leukemia cancer, Jurkat cell and breast cancer line, MCF-7.

The apoptogenic effect of *Sargassum muticum* stabilized gold nanoparticles appears to occur via the mitochondrial intrinsic pathway through caspases 3 and 9 activation (Namvar et al., 2015). Green synthesized gold nanoparticles using *Abelmoschus esculentus* (L.) pulp extract showed potent anti-proliferative efficacy against the Jurkat cell line at IC_{50} concentration of 8.17 mg ml^{-1} (Mollick et al., 2014).

Anticancer activity of *Nerium oleander*-conjugated gold nanoparticles studied against MCF-7 breast cancer cell line revealed that the stabilized AuNPs were highly efective for the apoptosis of cancer cells selectively (Barai et al., 2018).

The anticancer ability of the gold nano particles using *Camellia sinensis* (green tea), *Coriandrum sativum*, *Mentha arvensis*, *Phyllanthus amarus*, *Artabotrys hexapetalus*, *Mimusops elengi*, *Syzygium aromaticum*, *C. sinensis* (black tea) extracts was studied against MCF-7 cell at the IC_{50} concentration of 2µg/ml. (Priya and Iyer, 2015).

The present work highlights the apoptotic and oxidative stress producing potential of biogenic AuNPI3Cs in leukemia and breast cancer cell.

4.2 Materials and methods

4.2.1 Chemicals

Rosellpark Memorial Institute (RPMI-1640), Dulbecco's modified Eagle's medium (DMEM), Iscove's modified Dulbecco's medium (IMDM), fetal bovine serum (FBS) were procured from GIBCO. Antimytotic solution, 3-(4,5 dimethyl-2-thiazolyl)- 2,5-diphenyl-tetrazolium bromide (MTT), 2′,7′-dichlorodihydrofluorescein diacetate (H$_2$DCFDA), 4',6-diamidino-2-phenylindole (DAPI), propidium iodide (PI), rhodamine 123, phalloidin-iflour were

purchased from Sigma, Aldrich Co. St. Louis, US. Antibodies were obtained from Cell signalling technology, Beverly, MA, USA. Dimethyl sulfoxide (DMSO), agarose, phenol, chloroform, Tris buffer, ethidium bromide (EtBr), titron X-100, sodium dodecyl sulphate (SDS), sulfosalicylic acid, iso-amyl alcohol, ammonium acetate, RNAse, 5-fluorouracil,bis-acylaramide, poly-acylaramide, 4-Nitro blue tetrazolium chloride (NBT), 5-bromo-4-chloro-3'-indolyphosphate (BCIP) were procured from Merck, Millipore, (India) Pvt. Ltd., Mumbai.

4.2.2 Cancer cell lines and culture

Jurkat and MCF-7 cells were obtained from Chittaranjan National Cancer Institute (CNCI), Kolkata, India. IMDM and DMEM media were used for the culture of Jurkat and MCF-7 cells respectively. Both the medium were supplemented with 10% foetal bovine serum (FBS), 100 U ml^{-1}penicillin, 10 mg ml^{-1} streptomycin and 4 mM L-glutamine under 5% CO2 and 95% humidified atmosphere at 37˚C in an incubator. In the present study 1×10^6 ml^{-1} viable cells were used for different experiments.

4.2.3 Isolation and separation of of human lymphocytes

According to the method of Hudson and Hay, 1989 blood samples were collected from healthy human individual in 5 ml heparin-coated vacutainers. One ml of blood was taken with same amount of Histopaque 1077 (Sigma-Aldrich Co. LLC, US), the mixture was centrifuged at 2000 rpm for 30 min at room temperature. The upper monolayer buffy coat having lymphocytes were aspirated and transferred to a clean centrifuge tube and washed three times in phosphate buffer solution (PBS). Human lymphocytes (HLCs) were re-suspended in RPMI-1640 complete media containing 10% FBS and incubated for 24 h at 37°C under 5% CO$_2$ and 95% humidified atmosphere in a CO$_2$ incubator and used for the *in vitro* cytotoxicity assay.

4.2.4 Experimental design

Cells (1×10^6 cells/ml) were treated with different concentrations of I3C and AuNPI3Cs for *in vitro* cytotoxicity study against Jurkat and MCF-7cells. Control cells did not receive AuNPI3Cs. After the treatment schedule, cells were collected separately from the culture plates and centrifuged at 1200 rpm for 5 min at 4°C. Jurkat and MCF-7 cells were washed twice using 0.1 M PBS (pH 7.4). Jurkat, and MCF-7 cells (1×10^6 cells ml^{-1}) were treated with AuNPI3Cs at respective IC$_{50}$ dose for another experiments.

4.2.5 *In vitro* cytotoxicity study by MTT assay

The cytotoxicity of AuNPI3Cs was estimated by colorimetric assay using tetrazolium salt, 3-(4, 5-dimethylthiazol- 2-yl)-2,5-diphenyltetrazolium bromide (MTT) on HLC, Jurkat and MCF-7 cells. At first 1×10^6 cells/ml were seeded in IMDM, DMEM medium per well in a 96-well flat bottom culture plate with different concentrations of AuNPI3Cs (1, 2.5, 5, 10 and 25 µg ml^{-1}) for Jurkat and MCF-7 cells. The culture plates were incubated at 37°C and 5% CO_2 for 24 h. After incubation, 20 µl of MTT (5mg/ml in PBS) was added to each well and it was incubated for additional 3h at 37°C.

DMSO was added to solubilize the color of formazon and the optical density was noted at 540 nm by ELISA ANALYSER (Bio-Rad, Model 680) (Pradhan et al., 2016). All experiments were done thrice, and the proliferation of AuNPI3Cs treated Jurkat and MCF-7 cells were expressed as the percentage of cell viability.

% cell viability= [OD sample – OD control] $\times$100/OD control

4.2.6 Intracellular ROS measurement

The method was discussed (Roy et al., 2008) in chapter 3.

4.2.7 Estimation of reduced glutathione (GSH)

The method was described (Griffith, 1981) in chapter 3.

4.2.8 Determination of oxidized glutathione (GSSG)

Jurkat and MCF-7 cells were treated with AuNPI3Cs for 24h and washed with phosphate buffer. Then, 2 μl of 2-vinylpyidine was added to 100 μl of each sample and incubated for 1 h at 37 °C. The mixture was then deprotenized with 100 μl of 4gm % sulfosalicylic acid and centrifuged at 3000 rpm for 10 min to settle down the precipitated proteins. To the supernatant, 2 ml of 0.6 mM DTNB was added. The GSSG level was measured at 412 nm after the reaction of DTNB (Griffith 1980).GSSG contents were expressed as μg of GSSG mg^{-1} protein.

4.2.9 Cell morphology analysis by polarizing microscopy

After treatment, Jurkat and MCF-7 cells were washed with phosphate buffer and fixated with 2.5% glutaraldehyde in 0.1 M phosphate buffer (pH 7.4) for 1h at room temperature. Then, the samples were carefully washed with 0.1 M phosphate buffer (pH 7.4).

4.2.10 Chromatin condensation study by propidium iodide (PI) and 4′, 6′-diamidino-2-phenylindole dihydrochloride (DAPI) staining

Jurkat, MCF-7 (1×10^6cells ml^{-1}) cells were incubated with AuNPI3Cs at IC$_{50}$ dose for 24 h at 37°C and 5% CO$_2$. After washing, the cells were fixed by 70% chilled ethanol and incubated at ‒20°C for 2 h. After fixation, cells were washed and stained with RNAse-propidium iodide (PI) mixture (1mg ml^{-1}) and DAPI (1 μg ml^{-1}) at 37°C for 15 min. The cells were washed with phosphate buffer and placed under fluorescence microscope (LEICA DFC 295, Germany) to observe chromatin condensation (Prasad and Koch,2014).

4.2.11 Measurement of mitochondrial membrane potential (ΔΨm)

In brief, Jurkat and MCF-7 cells were treated with AuNPI3Cs at IC_{50} dose for 24 h. After treatment, cells were washed with fresh media and 1.5 μM rhodamine 123 was added to it and incubated for 15 min at 37ºC in a humidified chamber. After incubation, cells were again washed thrice with fresh media. The fluorescence intensity of rhodamine 123 was analysed for 2 min using a Hitachi F-7000 Fluorescence Spectrophotometer and an aliquot of cell suspension was also placed on a glass slide to observe under fluorescence microscopic (LEICA DFC295, Germany). Mitochondrial membrane potential of Jurkat and MCF-7 cells were expressed as a percentage of the control cells at an excitation wavelength of 493 nm and an emission wavelength of 522 nm (M'Bemba-Meka et al., 2006).

4.2.12 DNA fragmentation study by agarose gel electrophoresis

After 24 h treatment of AuNPI3Cs, cells were centrifuged at 1200 rpm to get the pellet. Washing with phosphate buffer saline (pH 7.4), the cells were again centrifuged at 1200-1500 rpm. Then 150-200 μl of lysis buffer (10 mM EDTA, 0.5% SDS, 10 mMTris base and 0.5 μg ml^{-1} proteinase K; pH 7.5) were mixed with the cell pellet and kept overnight. After 16 h, RNAse (0.5 μg ml^{-1}) solution was added to it. Then incubated for 2h at 37°C and isolated by phenol/chloroform/isoamyl alcohol (25:24:1 v/v/v) extraction method. DNA was then collected from the aqueous phase and precipitated by 7.5 M ammonium acetate and ice cold dehydrated ethanol. It was kept overnight at -20ºC and DNA was pelleted down at 10,000 rpm for 10 min and air dried. It was then dissolved in 20 μl of TE buffer (pH 7.4) and total 20 μl of DNA solution was loaded on 1.5% agarose gel containing 1 μg ml^{-1} ethidium bromide at 75 V (Gong et al., 1994). DNA fragments were visualized at UV light and then the image was captured by Gel-doc (Bio-Rad) apparatus.

4.2.13 Cell cycle analysis by flow cytometry

At first, cells were treated with AuNPI3Cs at IC_{50} dose for 24 h and after 24 h cells were centrifuged at 1000-1200 for 5 min. After washing, cells were fixed in 70% chilled ethanol (-20°C). After that samples were pelleted at 2000 rpm for 5 min and washed twice in ice-cold phosphate buffer. Then the cells were incubated with RNAse (10 mg ml^{-1}) solution for 1 h at 37ºC and then the cells were stained with propidium iodide (1mg ml^{-1}) at room temperature for 15 min at dark condition. The cells were then washed with PBS buffer and diluted with 500 µl PBS. Then, the cell cycle was analyzed using flow cytometer (BD FACSVerse) and Cell Quest software (Evans et al., 2000).

4.2.14 Cytoskeleton study by confocal microscopy

Briefly, after treatment schedule, the cells were washed with PBS buffer and fixed with 3-4% formaldehyde at room temperature for about ~10-30 min for the completion of fixation and again cells were washed 2-3 times in PBS. Then 0.1% triton-X 100 was added for permeabilization. They were rinsed 3 times in PBS and stained with 2µg ml^{-1} of 4′, 6′-diamidino-2-phenylindole dihydrochloride (DAPI) for 2 min at room temperature in the dark. After rinsing 6 times in PBS they were labelled with phalloidin-ifluor for 45 min at room temperature in the dark and rinsed in PBS. The slides were mounted with 50% glycerol and observed on laser-scanning confocal microscope setting at 405 nm for DAPI and 488 nm for phalloidin (Kntayya et al. 2018).

4.2.15 Western blot analysis

AuNPI3Cs treated Jurkat and MCF-7 cells (1×10^6 cells ml^{-1}) were exposed in RIPA buffer supplemented with cocktail protease inhibitor. Total protein were separated on SDS-PAGE and transferred to PVDF membranes. Membranes were pre-incubated with 5% non-fat dried milk protein solution.

Using specific primary antibodies against GAPDH (1: 1500 dilution), anti-Bcl2 (1:2000 dilution), anti-Bax (1:2000 dilution), anti-caspase-3(1:2000 dilution) the membranes were probed and then diluted in 5% BSA in Tris-buffered saline with Tween-20 (TBST) overnight at 4°C. After washing of specific protein bound PVDF membranes with TBST, ALP-conjugated suitable secondary antibodies (1:10000) was given and incubated. NBT-BCIP buffer was used to develop colour of protein bands (Mandal et al., 2006) and the picture was captured by Gel Doc (Bio-Rad).

4.3 Results

4.3.1 *In vitro* cytotoxicity by AuNPI3Cs

Treatment of AuNPI3Cs showed significant reduction of cellular viability in Jurkat and MCF-7 cells. At 50 μg ml^{-1} dose, Jurkat and MCF-7 cell viability was significantly decreased to 67.31% like the potent anticancer drug 5-FU (Figure 4.3). The IC$_{50}$ doses of AuNPI3Cs are 5, 4.9μg/ml whereas in case of I3C the value is 15, 13.27μg/ml in Jurkat and MCF-7 cell respectively.

(A)   **(B)**
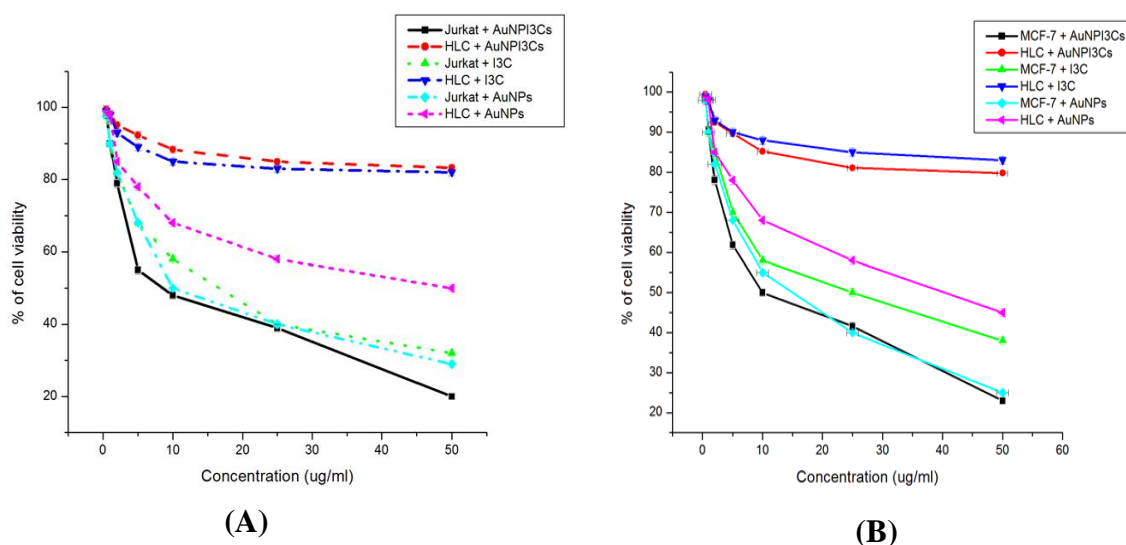
Figure 4.3 illustrates the effect of AuNPI3Cs on *in vitro* cytotoxicity against Jurkat cells (A) MCF-7 (B) and human lymphocyte cells (HLC).Cells were treated with AuNPI3Cs for 24 h at 37°C. Values are expressed as the means ±SEM of three experiments.

4.3.2 Oxidative stress in Jurkat and MCF-7 cells

The present study displayed decreased GSH and increased GSSG content significantly (p<0.001) in AuNPI3Cs treated Jurkat and MCF-7 cells (Figure 4.4a, 4.4b; 4.5a, 4.5b). Exposure to AuNPI3Cs for 24 h, enhanced ROS formation in Jurkat and MCF-7 cells was observed by the increase in fluorescence intensity of the DCF (Figure 4.6C, 4.6D) compared to control and the fluorescence images are significantly correlated to the above results (Figure 4.6).

(A)   **(B)**
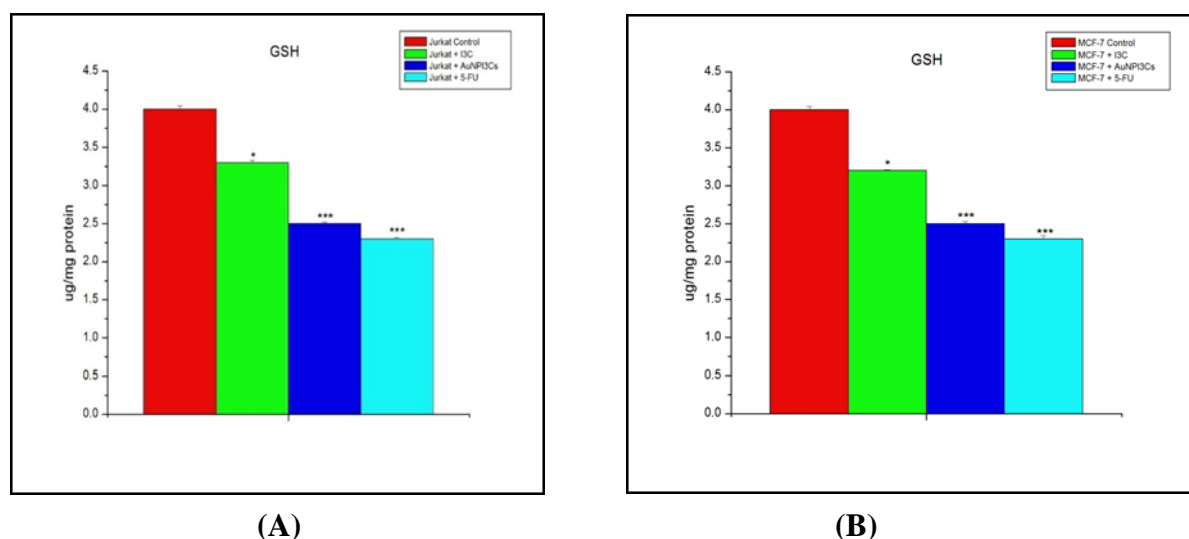
Figure 4.4 Intracellular reduced glutathione (GSH) level of Jurkat (A) and MCF-7 (B) cells. The level of GSH was expressed as μg of GSH mg^{-1} protein. Values are expressed as the Mean±SEM of three experiments. ; '*' indicates a statistically significant difference (p< 0.05) '***' indicates a statistically significant difference (p< 0.001), compared with Jurkat and MCF-7 control group.
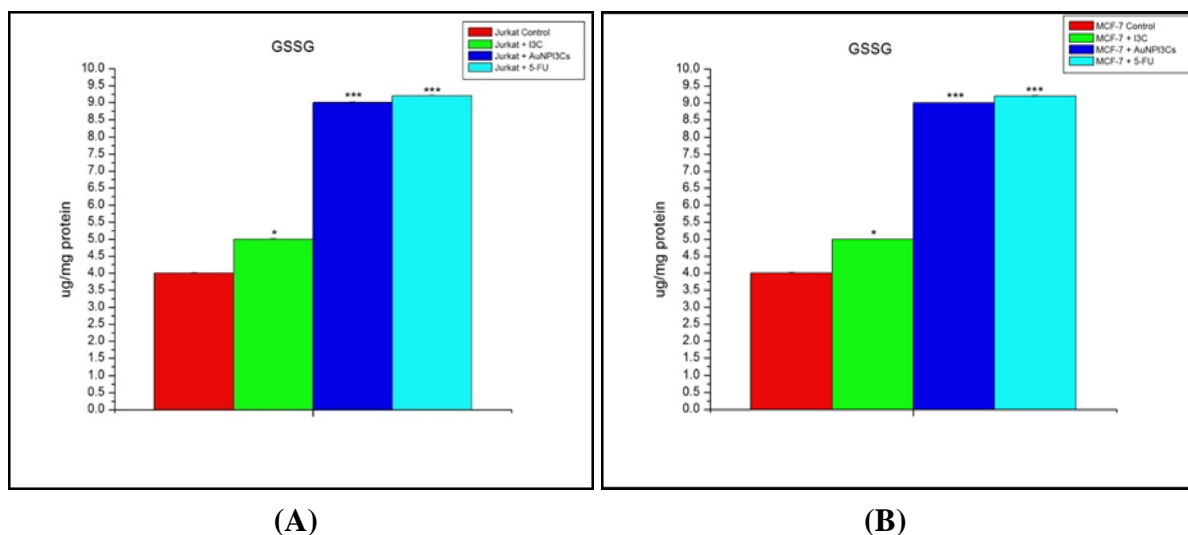
Figure 4.5 Intracellular oxidized glutathione (GSSG) level of Jurkat (A) and MCF-7 (B) cells. The level of GSSG was expressed as µg of GSSG mg^{-1} protein. Values are expressed as the Mean±SEM of three experiments. ; '*' indicates a statistically significant difference (p< 0.05) '***' indicates a statistically significant difference (p < 0.001), compared with Jurkat and MCF-7 control group.

(C)

(D)
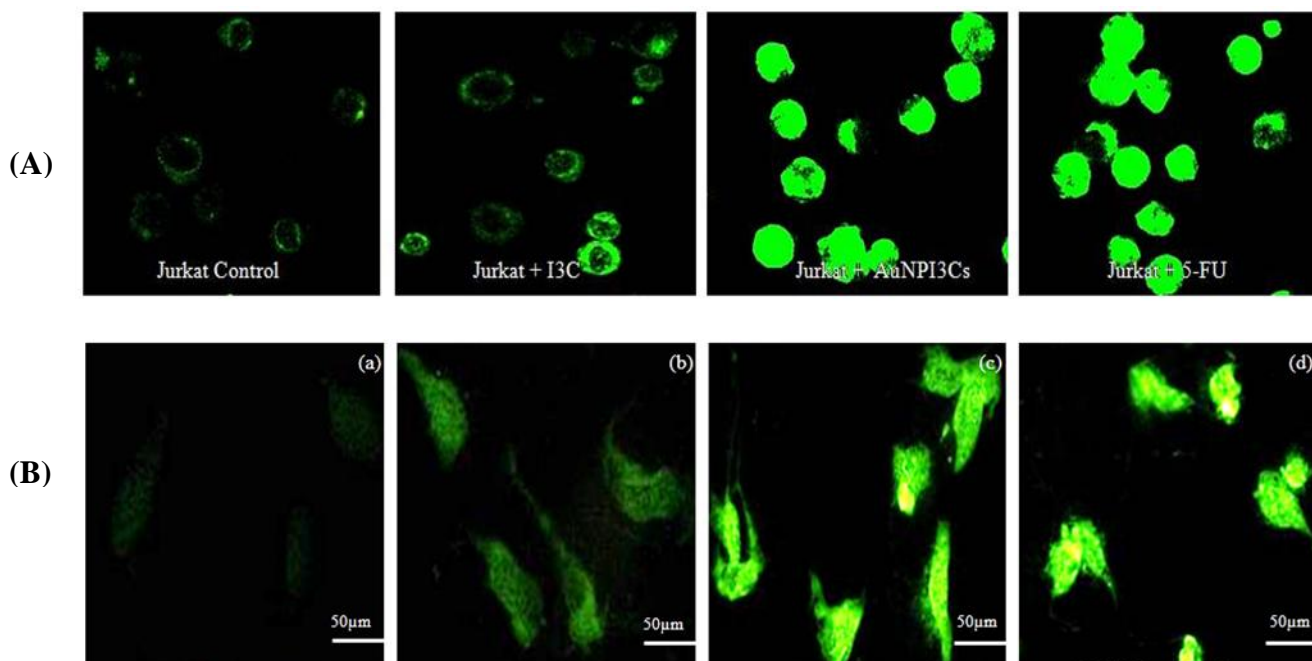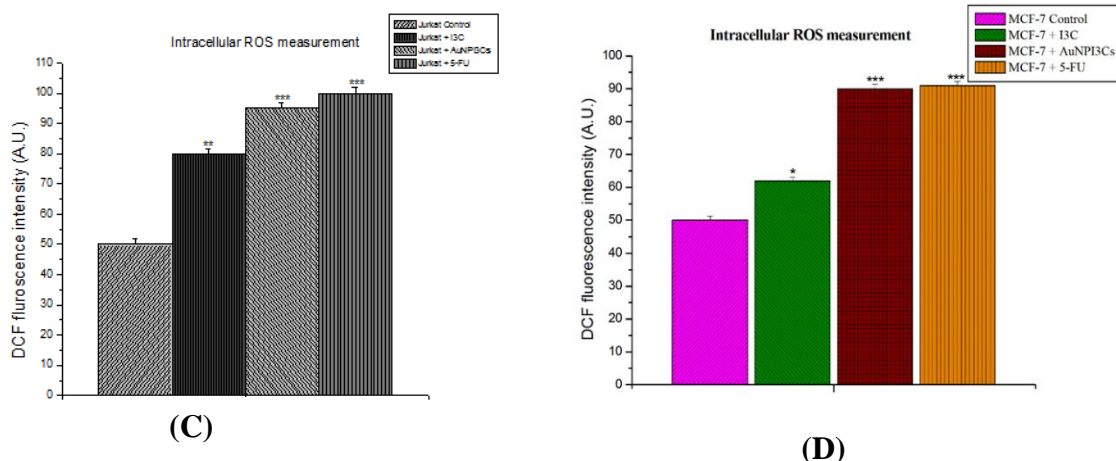
Figure 4.6 Intercellular ROS generation in Jurkat and MCF-7 cells after AuNPI3Cs treatment by H_2DCF_2DA staining using fluorescence microscopy.

(A) (a) Control Jurkat cells, (b) Jurkat cells treated with IC_{50} dose of I3C (c) Jurkat cells treated with IC_{50} dose of AuNPI3Cs and (d) 5-FU treated Jurkat cells (B) (a) Control MCF-7 cells, (b) MCF-7 cells treated with IC_{50} dose of I3C (c) MCF-7 cells treated with IC_{50} dose of AuNPI3Cs and (d) 5-FU treated MCF-7 cells. Effects of AuNPI3Cs and 5-FU on induction of reactive oxygen species (ROS) in Jurkat (C) and MCF-7(D) cell lines.

4.3.3 Cellular morphological analysis by phase contrast

Phase contrast microscopic observations revealed morphological alterations of Jurkat and MCF-7 cells respectively after exposure to AuNPI3Cs. Morphological changes, including membrane blebbing and other changes in the cancer cell membrane, such as loss of attachment and cell shrinkage, are the early stages of apoptosis that can be analyzed by phase contrast microscopy (Figure 4.7).
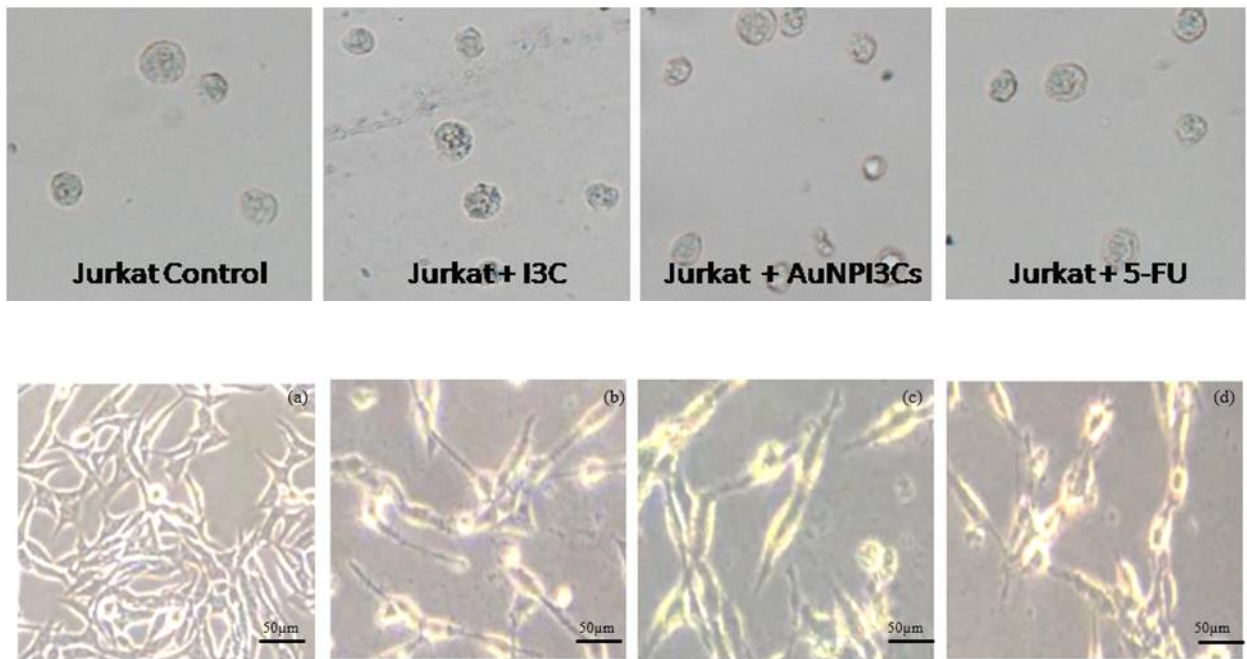
Figure 4.7: Photomicrographs of morphology of I3C- and AuNPI3Cs-treated apoptotic Jurkat and MCF-7 cells under phase contrast microscope; a) Jurkat/MCF-7 Control, b) Jurkat/MCF-7 + I3C, c) Jurkat/MCF-7 + AuNPI3Cs, d) Jurkat/MCF-7 + 5-FU

4.3.4 Chromatin condensation study by AuNPI3Cs

Chromatin condensation study showed bright red (Figure 4.8) and blue punctuated nuclei (Figure 4.9) in AuNPI3Cs treated groups after PI and DAPI staining respectively.
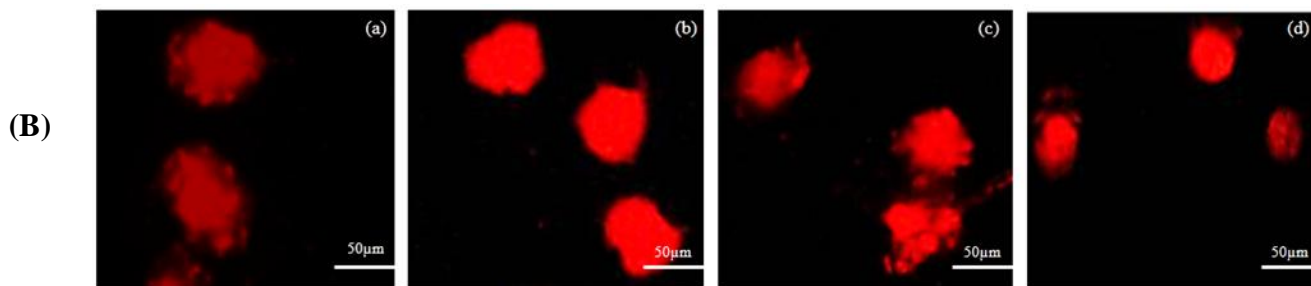
(A)

82

(B)
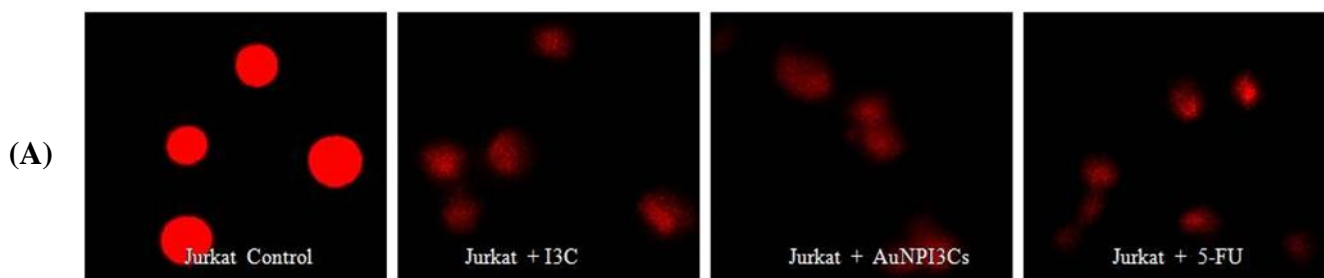
Figure 4.8 Fluorescence microscopic observation of (A) Jurkat (B) and MCF-7 cells treated with IC_{50} dose of AuNPI3Cs for 24 h and stained with PI to detect chromatin condensation. A. (a) Control Jurkat cells, (b) Jurkat cells treated with IC_{50} dose of I3C (c) Jurkat cells treated with IC_{50} dose of AuNPI3Cs and (d) 5-FU treated Jurkat cells. B. (a) Control MCF-7 cells, (b) MCF-7 cells treated with IC_{50} dose of I3C (c) MCF-7 cells treated with IC_{50} dose of AuNPI3Cs and (d) 5-FU treated MCF-7 cells.
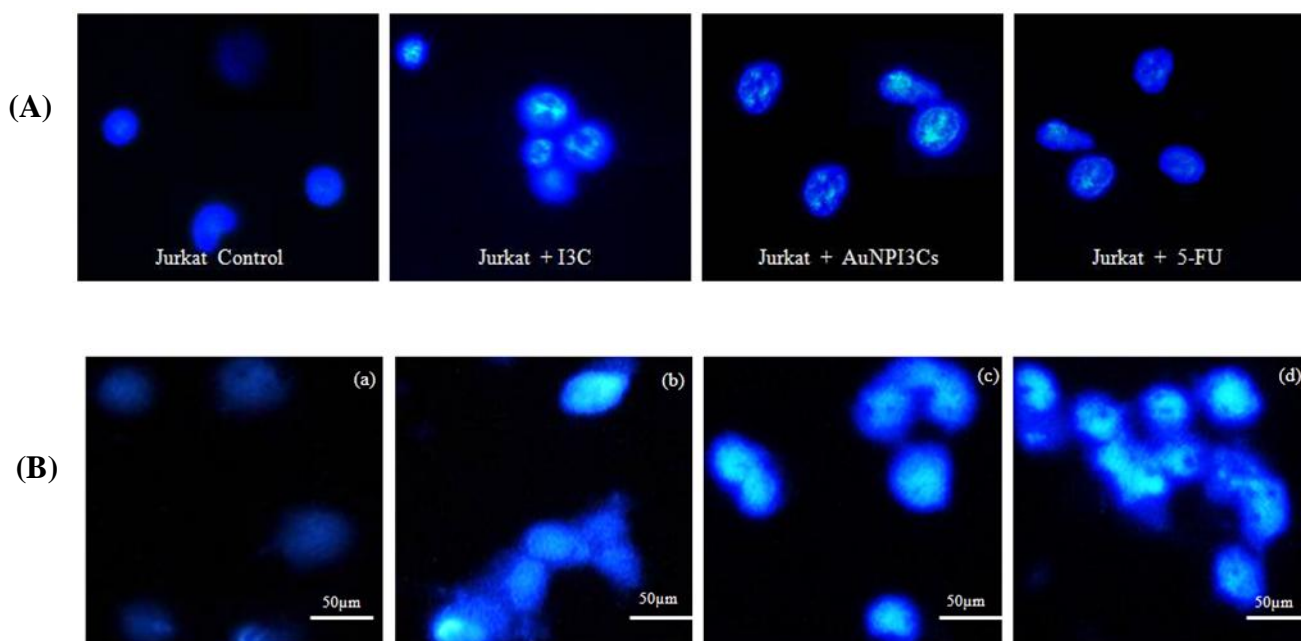
(A)

(B)

Figure 4.9 Chromatin condensation in Jurkat and MCF-7 cells treated with IC_{50} dose of AuNPI3Cs for 24 h after staining with DAPI. (A) a) Jurkat Control, b) Jurkat + I3C, c) Jurkat + AuNPI3Cs, d) Jurkat + 5-FU. (B) a) MCF-7 Control, b) MCF-7 + I3C, c) MCF-7 + AuNPI3Cs, d) MCF-7 + 5-FU.

4.3.5 Effect on mitochondrial membrane potential

Mitochondrial membrane potential was expressed as rhodamine123 fluorescence intensity (Figure 4.10). Rhodamine-123 fluorescence intensity decreased significantly in AuNPI3Cs treated Jurkat and MCF-7 cells.
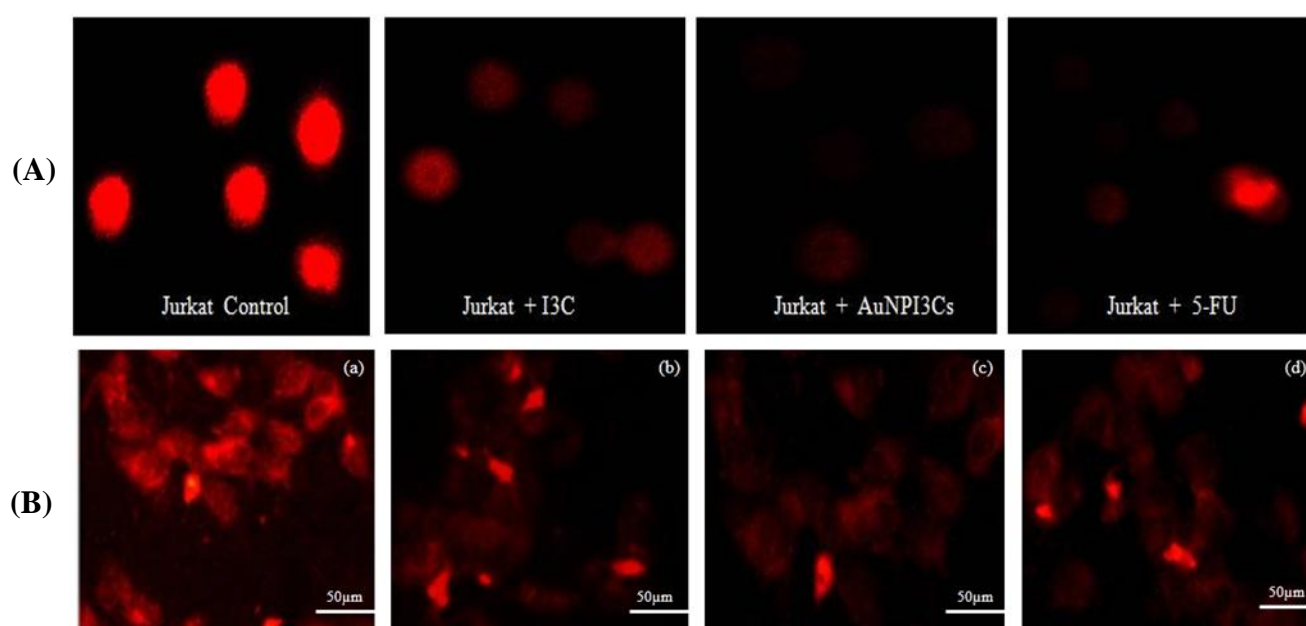

Figure 4.10a: Mitochondrial membrane potential by Rhodamine 123 staining using fluorescence microscopy in AuNPI3Cs-treated Jurkat and MCF-7 cells. (A) a) Jurkat Control, b) Jurkat + I3C, c) Jurkat + AuNPI3Cs, d) Jurkat + 5-FU. (B) a) MCF-7 Control, b) MCF-7 + I3C, c) MCF-7 + AuNPI3Cs, d) MCF-7 + 5-FU.
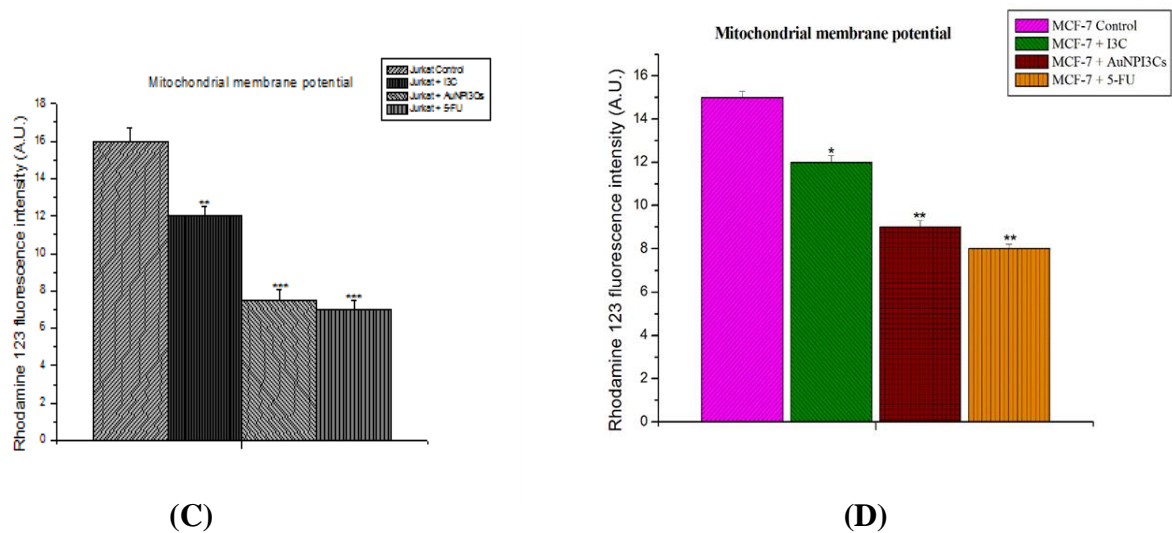
(C)　　　　　　　　　　　　　　**(D)**

Figure 4.10b: Measurement of Rhodamine 123 fluorescence intensity of Jurkat (C) and MCF-7 (D) cells using fluorescence spectrophotometer. Values are expressed as the mean± SEM of three experiments; '**' indicates a statistically significant difference ($p < 0.01$) '***' indicates a statistically significant difference ($p < 0.001$), compared to the control group.

4.3.6 Effect of AuNPI3Cs on DNA fragmentation

Agarose gel electrophoresis study revealed smear like DNA pattern in AuNPI3Cs treated Jurkat and MCF-7cells (Figure 4.11).
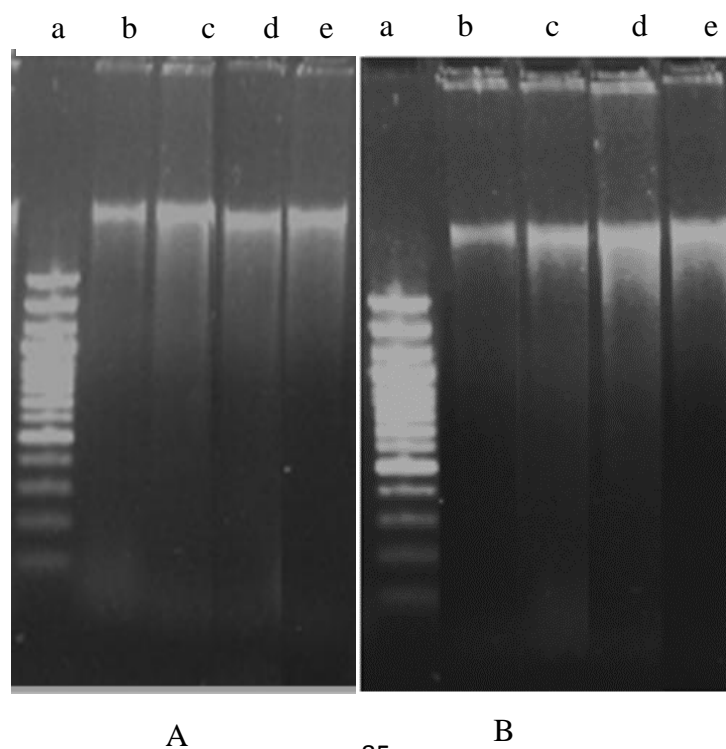

A　　　　　　　　　　　　　　B

Figure 4.11 DNA fragmentation study in Jurkat and MCF-7 cells by agarose gel electrophoresis. (A. a: 100 bp DNA Ladder, b: DNA of Jurkat control group, c: DNA of I3C treated Jurkat cells, d: DNA of AuNPI3Cs treated Jurkat cells, e: DNA of 5-FU treated Jurkat cells. B. a: 100 bp DNA Ladder, b: DNA of MCF-7 control group, c: DNA of I3C treated MCF-7 cells, d: DNA of AuNPI3Cs treated MCF-7 cells, e: DNA of 5-FU treated MCF-7 cells).

4.3.7 Cell cycle arrest by AuNPI3Cs

AuNPI3Cs exhibited cell cycle arrest at G_0/G_1 phase in both cell lines (Figure 4.12).
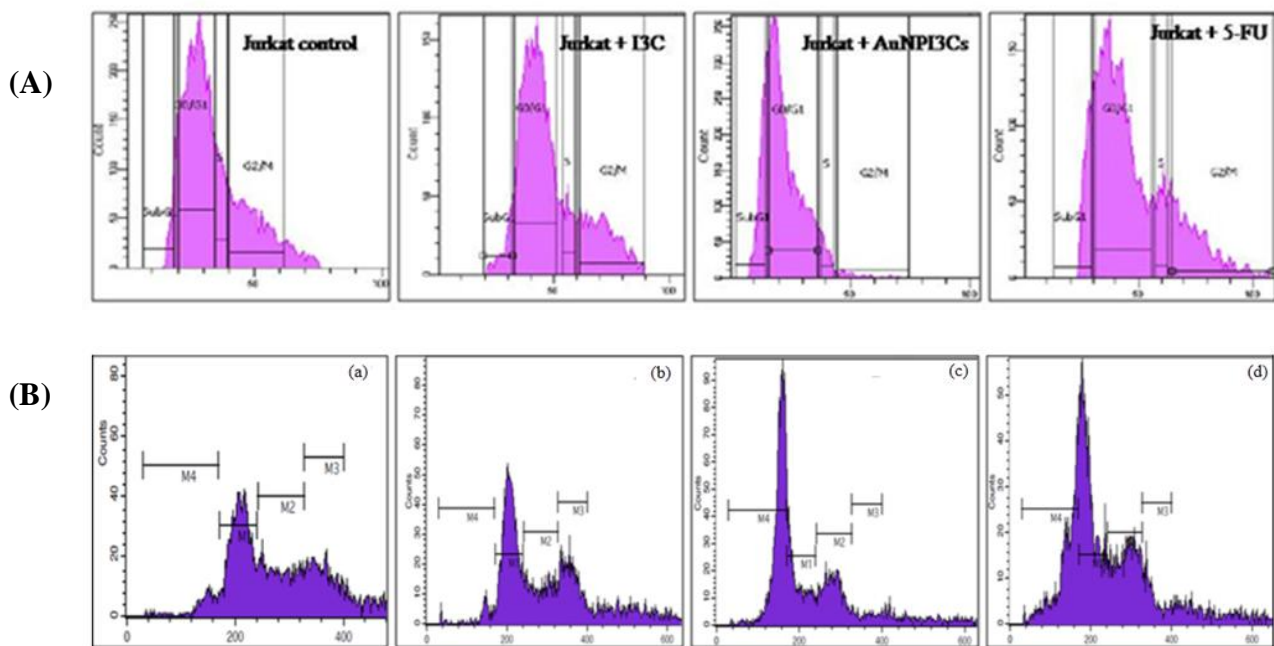

Figure 4.12 Analysis of cell cycle arrest by flow cytometry. Cells were treated with AuNPI3Cs and 5-FU for 24 h, stained with PI and flow cytometry was done to observe the cell distributions among sub-G_0, G_0/G_1, S and G2/M phases. A, (a) Jurkat Control, (b) I3C-treated Jurkat cells, (c) AuNPI3Cs -treated Jurkat cells and (d) 5-FU treated Jurkat cells. B.

(a) MCF-7 Control, (b) I3C-treated MCF-7 cells, (c) AuNPI3Cs-treated MCF-7 cell and (d) 5-FU treated MCF-7 cell.

4.3.8 Cytoskeleton study by AuNPI3Cs on MCF-7 cells

Phalloidin/DAPI double staining assay was performed to detect apoptotic cytoskeletal damage in MCF-7 cell by confocal laser microscopy (Figure 4.13).
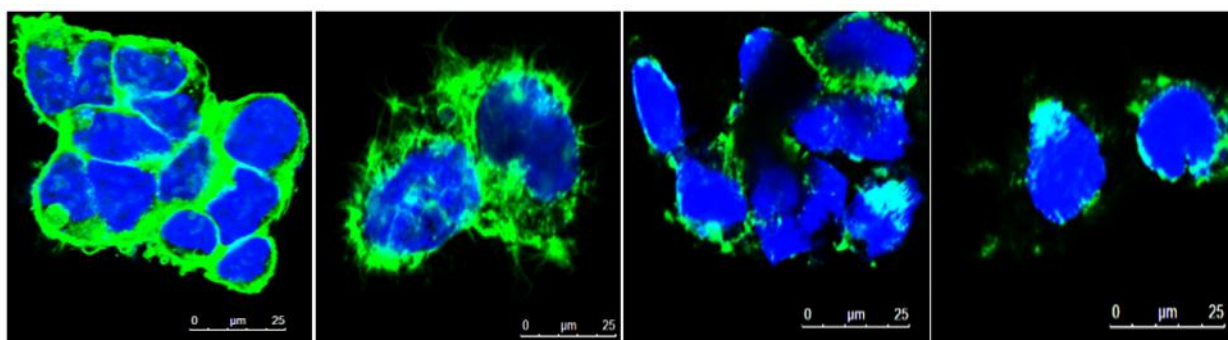

Figure 4.13: Photomicrographs of cytoskeletal destruction in apoptotic MCF-7 cells treated with I3C and AuNPI3Cs under polarizing microscope. a) MCF-7 control, b) MCF-7 + I3C, c) MCF-7 + AuNPI3Cs, d) MCF-7 + 5-FU.

4.3.9 Effect on expression of apoptotic proteins

Down regulation of Bcl-2 and up regulation of Bax and caspase-3 proteins were revealed in AuNPI3Cs-treated Jurkat and MCF-7 cells by Western blot analysis (Figure 4.17).
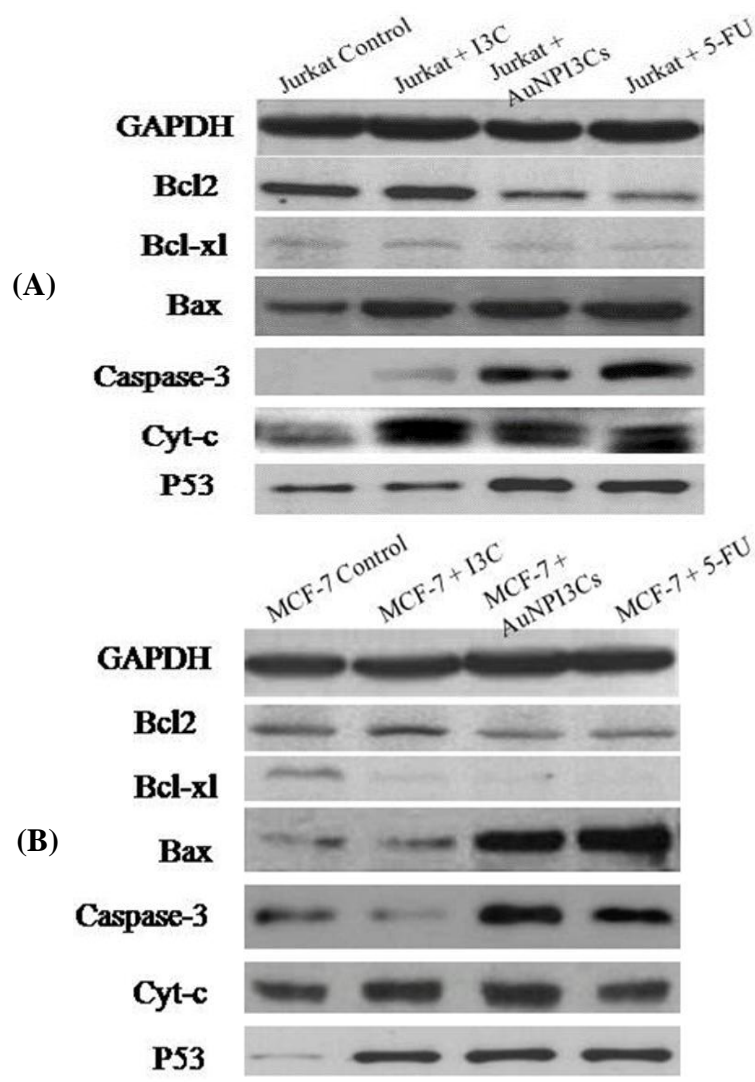
Figure 4.14. Western blot analysis of proapoptotic and antiapoptotic proteins in Jurkat (A) and MCF-7 (B) cells treated with I3C and AuNPI3Cs. GAPDH is used as loading control.

4.4 Discussion

Cancer is a major public health problem in both developed and developing countries. In this study, leukemic and breast cancer cell line were used to determine the anticancer effects of gold nanoparticles using indole-3-carbinol (AuNPI3Cs).

At IC_{50} value (5.55 µg ml^{-1}) of AuNPI3Cs, no trace of cytotoxicity was observed in human lymphocytes. The IC_{50} dose of AuNPI3Cs is 7.5µg/ml whereas in case of I3C the value is

13.27µg/ml on MCF-7 cell. These data created interest as it suggested that AuNPI3Cs were more toxic to cancer cells compared to normal cells. However, a significant number of patients develop tamoxifen-resistance and experience severe side effects (Lazarus et al., 2009).

GSH is a scavenger of free radicals such as reactive oxygen species (ROS) and reactive nitrogen species (RNS) and in its presence, there is no accumulation of the oxidants. Since glutathione is a powerful intracellular antioxidant (Prasad and Rao, 2012), it was expected that if AuNPI3Cs were working via a redox mechanism then AuNPI3Cs were possibly exerting its anticancer activity on Jurkat and MCF-7 cells and generates ROS which resulted cell death. ROS are greatly active and have a pivotal role in cell signaling leading to oxidative cell injury due to their unpaired valence shell electrons (Davis et al., 2009). Exposure to AuNPI3Cs enhanced ROS formation in Jurkat and MCF-7 cells in terms of DCF fluorescence intensity (Figure 4.6) and respective fluorescence images (Figure 4.6) revealing its anticancer potential towards Jurkat and MCF-7 cells.

Morphological changes, including membrane blebbing are the early stages of apoptosis and that was assessed by polarizing microscopy. As shown in Figure 4.7, the figure reveals AuNPI3Cs induced membrane blebs and disruption in Jurkat and MCF-7 cells compared to the control cells. Our findings revealed that the occurrence of morphologically altered cells was in highest number in AuNPI3Cs treated Jurkat and MCF-7 cells.

 The effect of AuNPI3Cs on the induction of apoptosis in human T-cell leukemia, Jurkat and breast cancer, MCF-7 cells was also assessed by DAPI and PI staining (Chen et al., 2008). The nuclear changes observed in AuNPI3Cs treated Jurkat and MCF-7 cells exhibited typical morphological changes of apoptosis, including cell shrinkage, plasma membrane blebbing, chromatin condensation, and nuclear fragmentation, compared to control group. An increase in early apoptotic populations of Jurkat and MCF-7 cells was observed when treated with

AuNPI3Cs. Appearance of crescents around the periphery of the nucleus or the entire chromatin as featureless, bright blue or bright red spherical beads, typical of apoptosis (Figure 4.8,4.9) was observed in MCF-7 cells after treatment with I3C and AuNPI3Cs for 24 h supported by the study of Kntayya et al.,2018.

To determine the role of mitochondria in AuNPI3Cs-induced apoptosis, the effects of AuNPI3Cs was investigated on MMP ($\Delta\Psi$ m) using Rh123. Reduction of $\Delta\Psi$ m in mitochondria is an indication of apoptosis. AuNPI3Cs significantly decreased $\Delta\Psi$ m in Jurkat and MCF-7 cells at its IC_{50} dose (Figure 4.10). It may be due to the less ATP synthesis and maintenance of ATP levels, resulting to apoptosis (Adrie et al., 2001). It was reported earlier that after nanoparticles exposure, decreased mitochondrial membrane potential leads to increased production of reactive oxygen species (ROS) which ultimately leads to cell death via apoptosis in treated cells (Zamzami et al.,1995).

DNA fragmentation study by agarose gel electrophoresis was done to determine whether the death of both Jurkat and MCF-7 cells had occurred due to the apoptotic effect of AuNPI3Cs treatment or not. Smear like pattern of DNA was noticed in treated group, however untreated cells showed intact DNA band and both the cancer cell lines were sensitive to AuNPI3Cs at their respective IC_{50} dose levels (Figure 4.11).

Many chemotherapeutic drugs induce apoptosis-mediated cell death by disrupting nuclear DNA (Bai and Cederbaum, 2003). In cancer cells, genomic DNA damaging ability of antitumor drugs leads to apoptosis (Jamieson and Lippard, 1999). Cancer cells exposed to AuNPI3Cs showed an increased G0/G1 phase cell population ($p<0.05$) compared to indole-3-carbinol treated group (Figure 4.12). This could suggest that AuNPI3Cs treated Jurkat and MCF-7 cells had undergone cell cycle arrest at G0/G1 phase.

Cells in the control groups populated very well and grew strongly at a high density. Comparing to the intact and polygonal shape in the control group, cells exposed to

AuNPI3Cs and 5-FU showed shrink margin and loss of contact with the adjacent cells. Phalloidin/DAPI cytological investigations explicated that the membrane instability and cytoskeleton was affected by AuNPI3Cs and 5-FU (Cao et al., 2018).

In order to understand the mechanism by which AuNPI3Cs induces apoptosis, we investigated the changes in the expression levels of apoptotic proteins. Results showed that AuNPI3Cs treatment led to significant upregulation of proapoptotic proteins like BAX and Caspase 3 (Figure 4.14). By immunoblotting analysis, we found that AuNPI3Cs treatment led to significant down-regulation of antiapoptotic proteins like Bcl2 and Bclxl, suggesting the activation of intrinsic pathway of apoptosis. Apoptosis involves a complex network of protein-protein interactions that essentially rely on the balance between the antiapoptotic (Bcl2, Bcl-xl) and proapoptotic (BAX) proteins (Ferri and Kroemer, 2001). Thus, our results suggest that AuNPI3Cs activate the mitochondrial pathway of apoptosis in Jurkat and MCF-7 cells.

4.5 Conclusion

It can be concluded from the above results that AuNPI3Cs have the potent capability of antiproliferative, antineoplastic and anti-apoptotic activity against Jurkat and MCF-7 cells.

Increase in ROS generation and decrease in mitochondrial membrane potential as well as DNA fragmentation and cell cycle arrest at G0/G1phase indicated that AuNPI3Cs exert cytotoxic effect through the induction of apoptosis. This apoptotic induction was confirmed by Western blot analysis which showed up-regulation of pro-apoptotic proteins and down regulation of anti-apoptotic proteins in AuNPI3Cs treated Jurkat and MCF-7 cells. Overall, the present study reveals that AuNPI3Cs possess significant anticancer activity against Jurkat and MCF-7 cell lines and AuNPI3Cs may be a novel promising therapeutic agent in the treatment of human T-cell leukemia and breast cancer in future.